Supplementary Information (SI) for Journal of Materials Chemistry A.

This journal is © The Royal Society of Chemistry 2025

Supporting Information for

In-situ surface reconstruction of silver leads to competent activity for the electrocatalytic hydrogenation of 5-hydroxymethylfurfural

Dalong Qu,[a] Nan Jiang,*[a] and Yujie Sun*[b]

[a] Department of Chemistry and Chemical Engineering, Guizhou University, Guiyang 550025, Guizhou, China. E-mail: njiang@gzu.edu.cn.

[b] Department of Chemistry, University of Cincinnati, Cincinnati 45221, Ohio, United States. E-mail: yujie.sun@uc.edu

*Corresponding authors: Nan Jiang and Yujie Sun

E-mail: njiang@gzu.edu.cn; yujie.sun@uc.edu

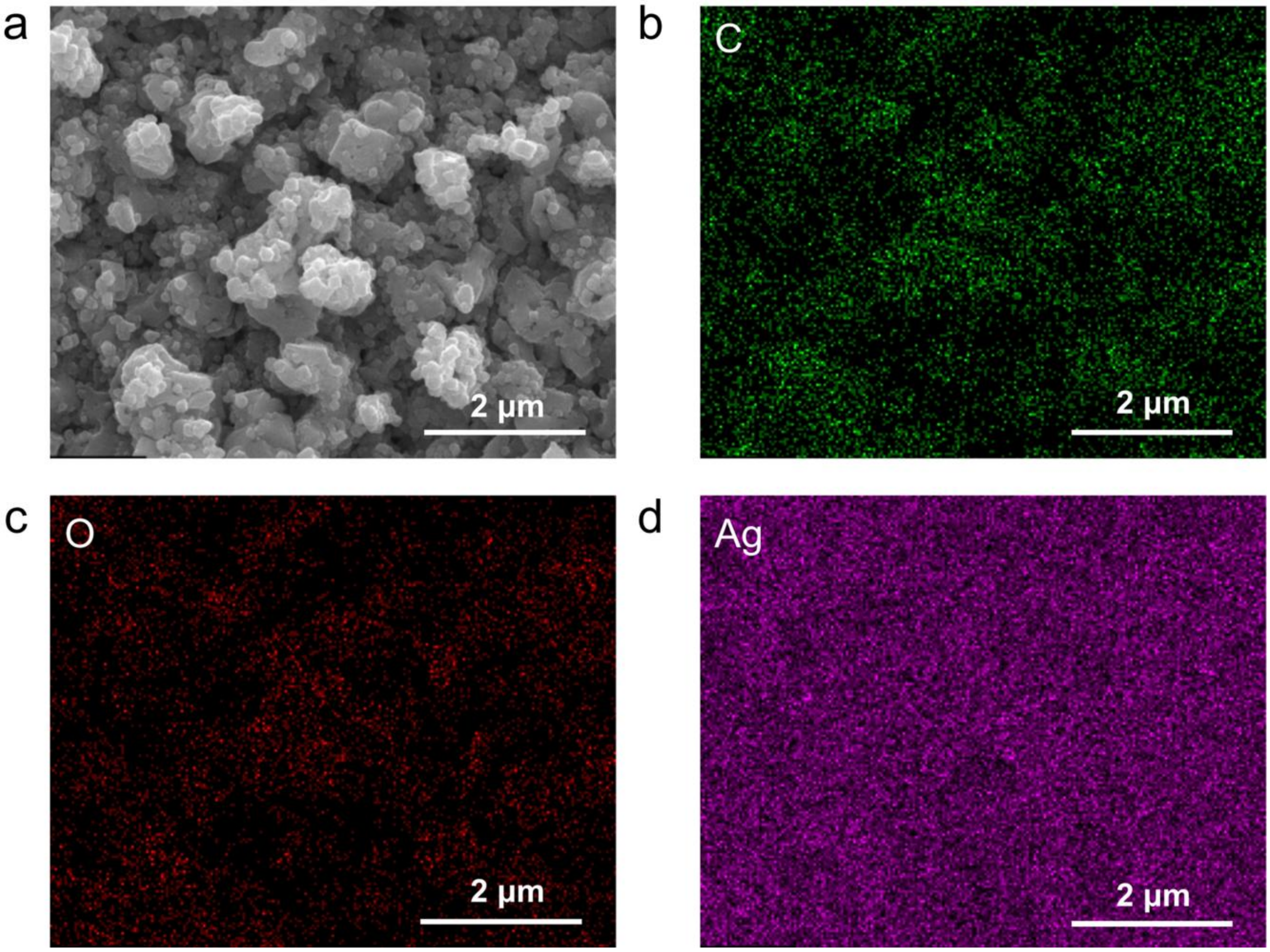

Fig. S1 (a) SEM image of AD-Ag. (b-d) Corresponding elemental mappings.

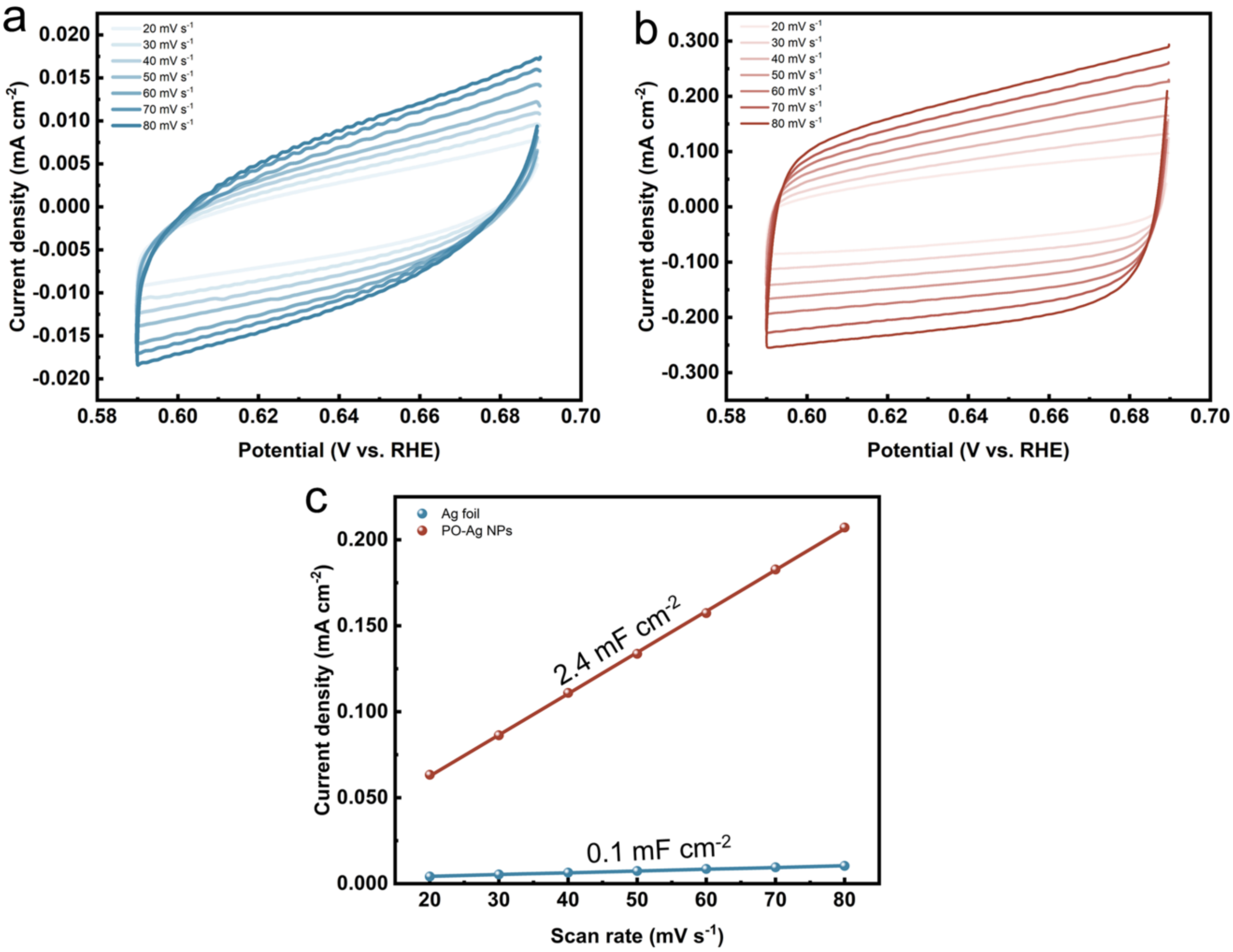

Fig. S2 CV curves of (a) Ag foil and (b) PO-Ag NPs performed in a 1 M borate buffer solution at scan rates from 20 to 80 mV s^{-1}. (c) Scan rate dependence of the current densities of Ag foil and PO-Ag NPs (dotted lines) at 0.59 ~ 0.69 V vs. RHE and their corresponding linear fittings (solid lines).

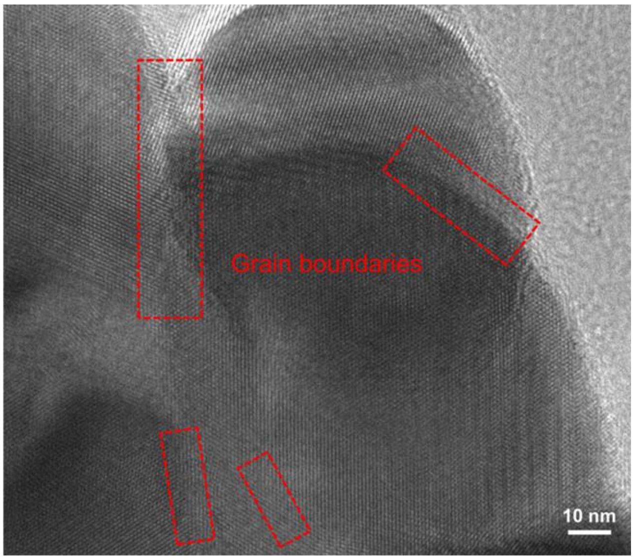

Fig. S3 TEM image of PO-Ag NPs.

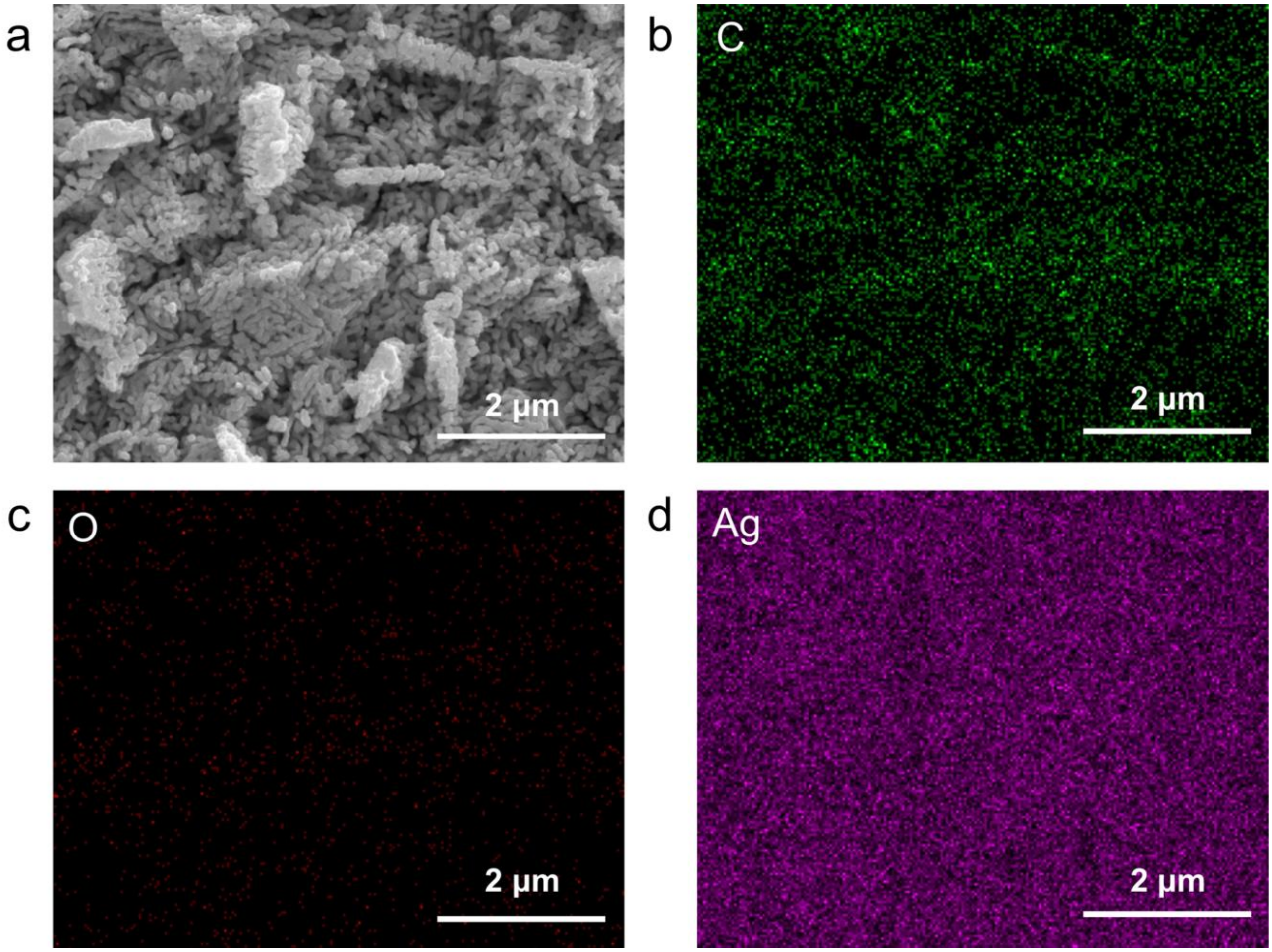

Fig. S4 (a) SEM image of PO-Ag NPs. (b-d) Corresponding elemental mappings.

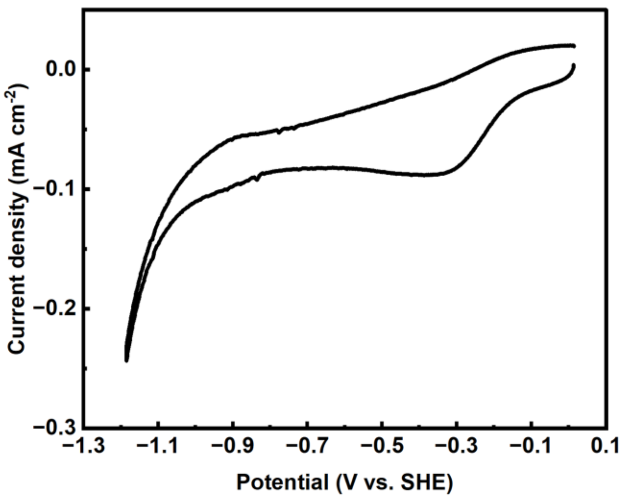

Fig. S5 CV curve of Ag foil in 0.5 M $KHCO_3$ saturated with N_2.

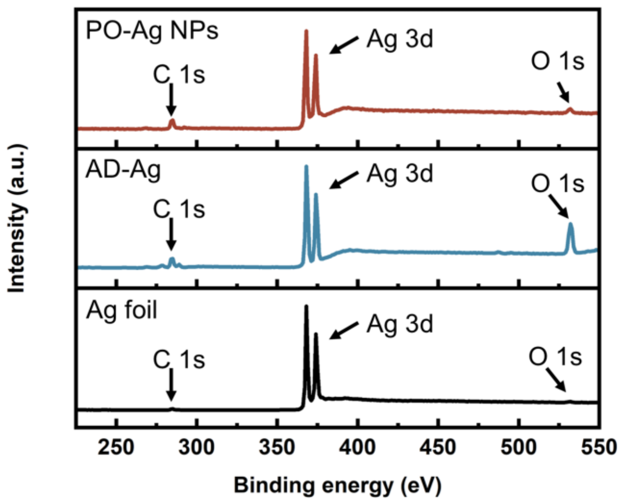

Fig. S6 XPS survey spectra of Ag foil, AD-Ag, and PO-Ag NPs.

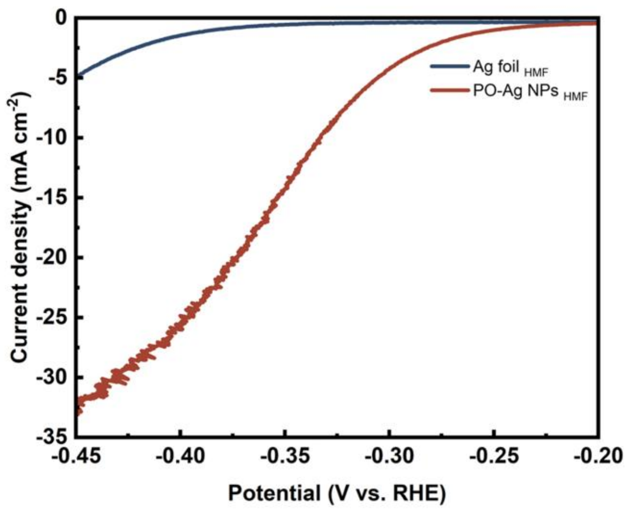

Fig. S7 LSV curves for Ag foil and PO-Ag NPs in 1 M borate buffer solution in the presence of 50 mM HMF.

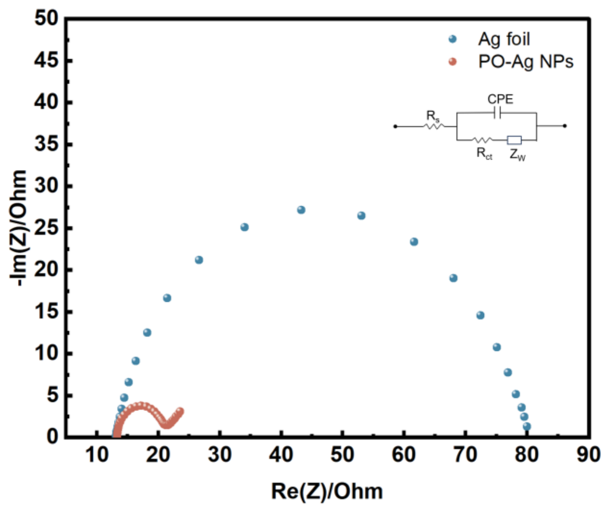

Fig. S8 Nyquist plots for HMF hydrogenation over an Ag foil and PO-Ag NPs at –0.41 V vs. RHE in the presence of 50 mM HMF.

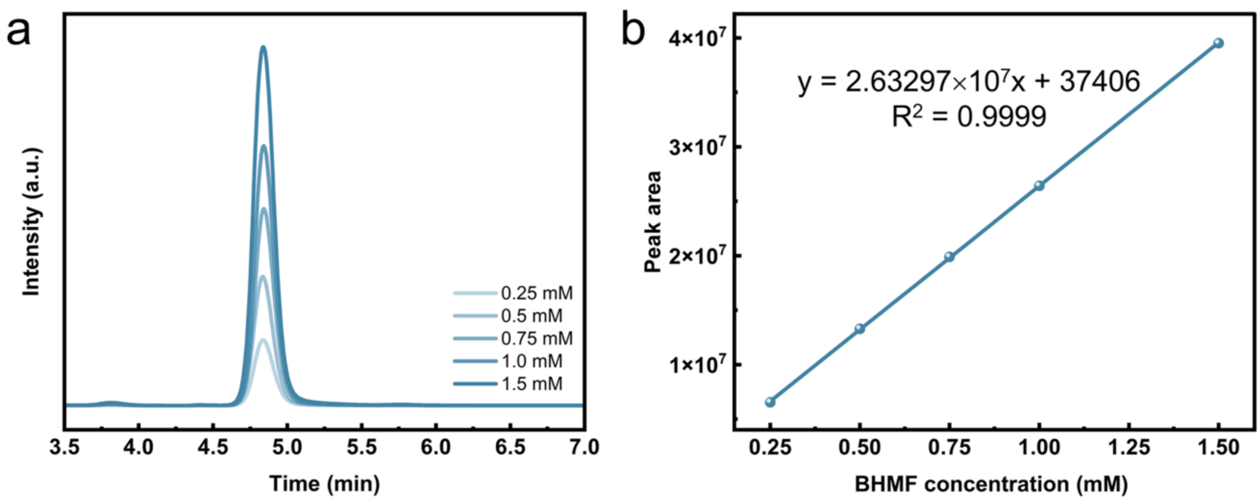

Fig. S9 (a) HPLC traces of the commercial BHMF at different concentrations. (b) Corresponding calibration plots of the commercial BHMF.

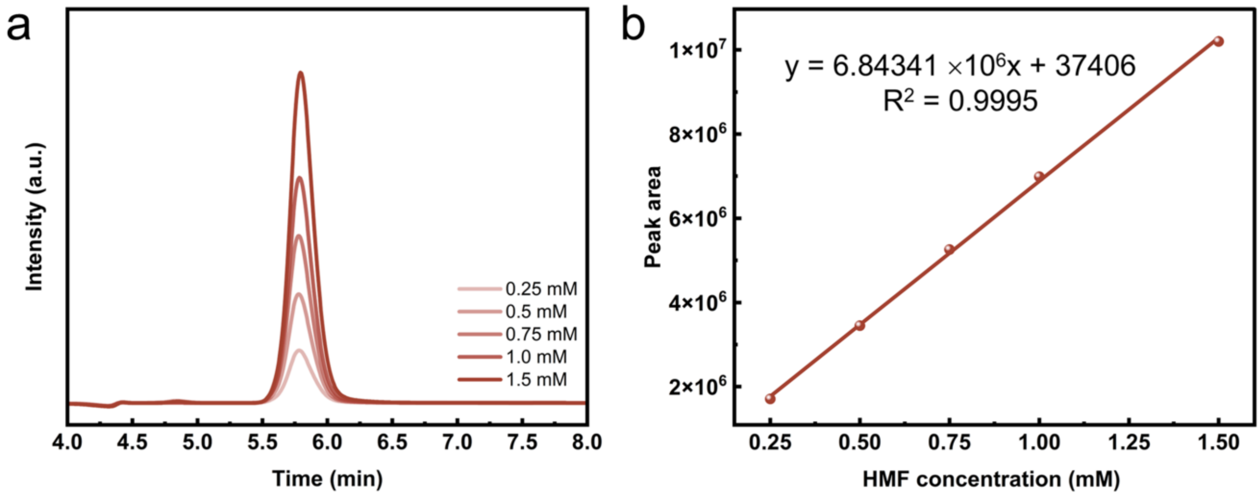

Fig. S10 (a) HPLC traces of the commercial HMF at different concentrations. (b) Corresponding calibration plots of the commercial HMF.

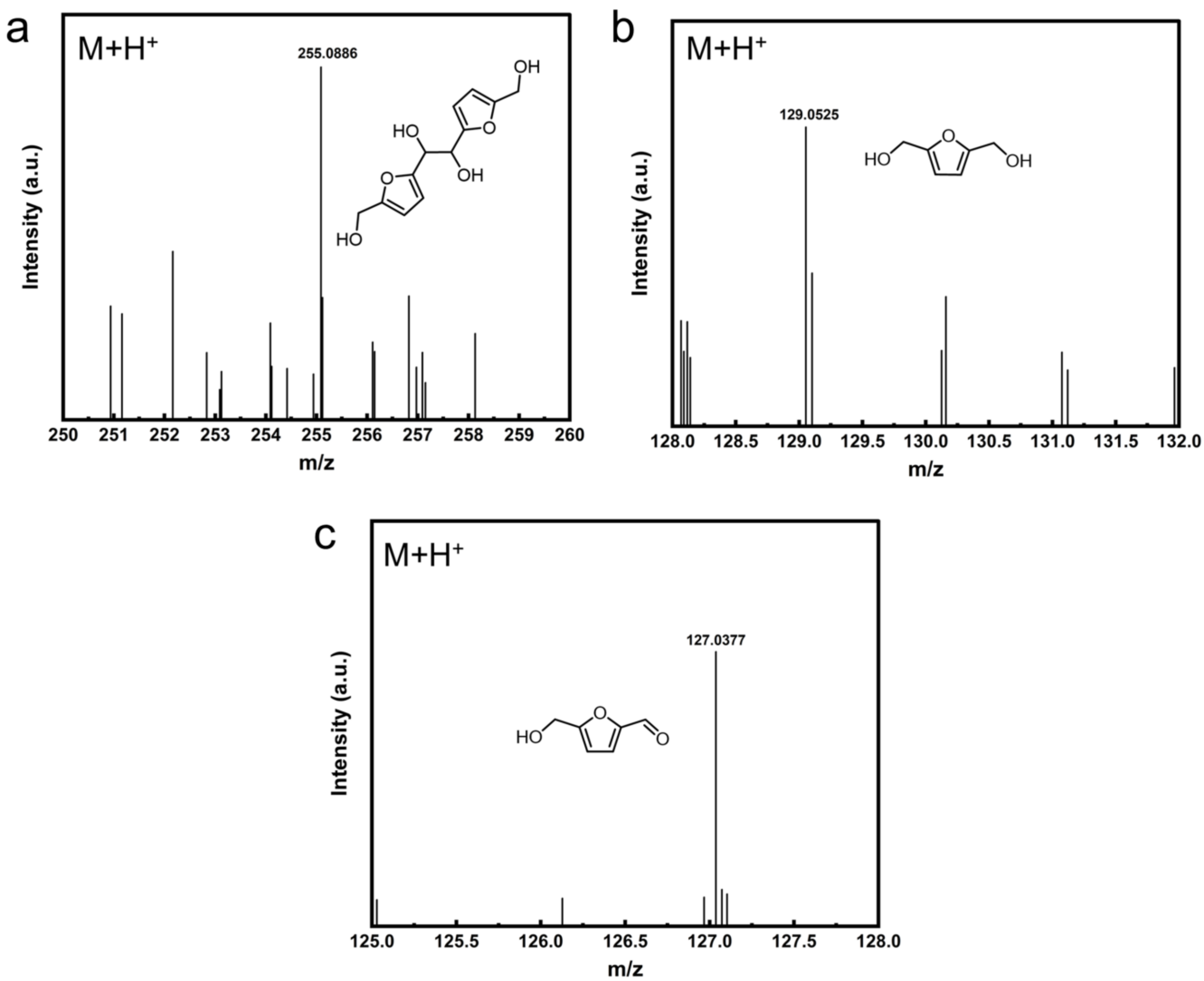

Fig. S11 LC-MS spectra of (a) BHH, (b) BHMF, and (c) HMF.

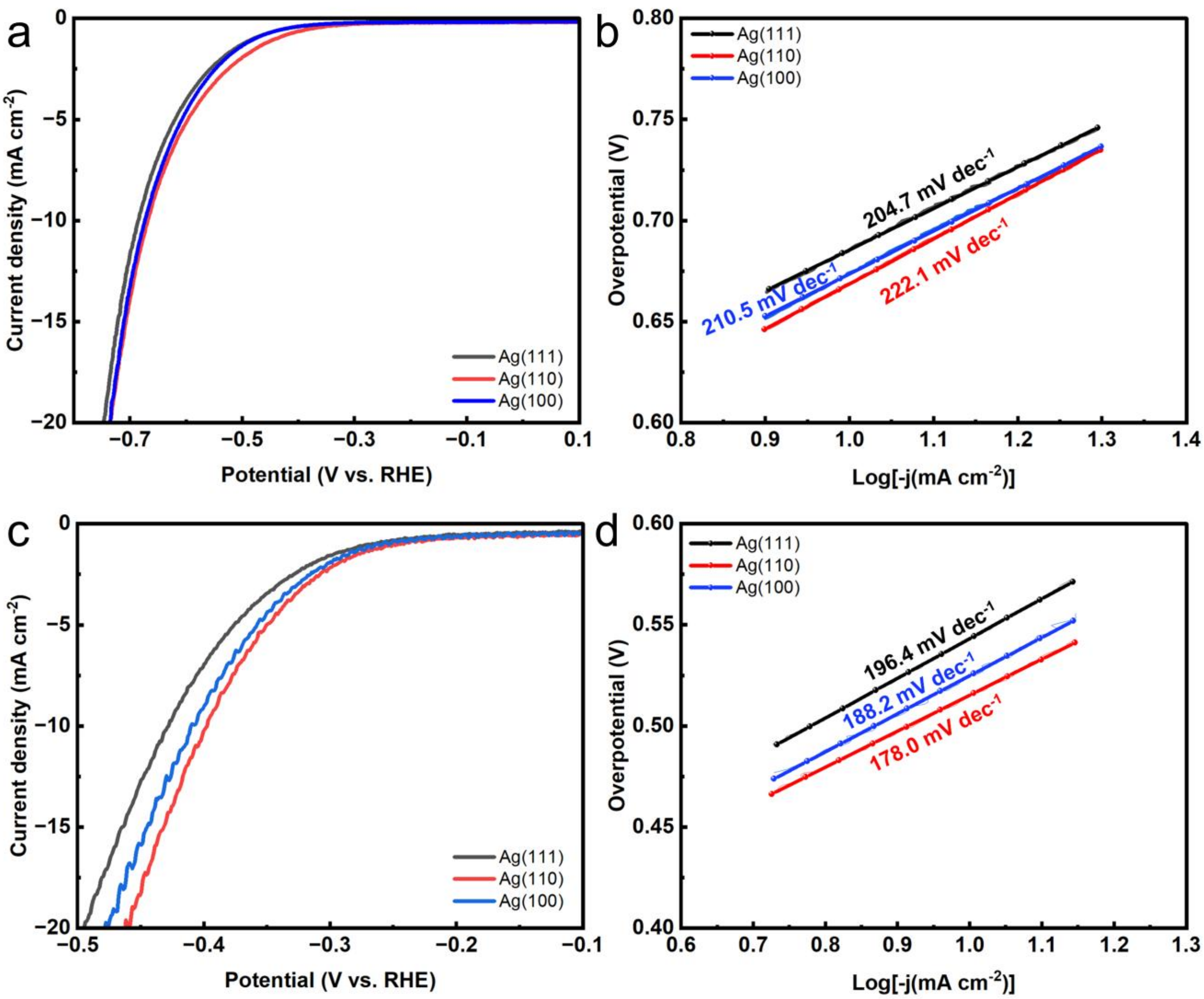

Fig. S12 (a) LSV curves of Ag(111), Ag(110), and Ag(100) in 1 M borate buffer solution at a scan rate of 5 mV s^{-1}. (b) Tafel slopes for HER over Ag(111), Ag(110), and Ag(100). (c) LSV curves of Ag(111), Ag(110), and Ag(100) in 1 M borate buffer solution with 50 mM HMF at a scan rate of 5 mV s^{-1}. (d) Tafel slopes for HMF hydrogenation over Ag(111), Ag(110) and Ag(100).

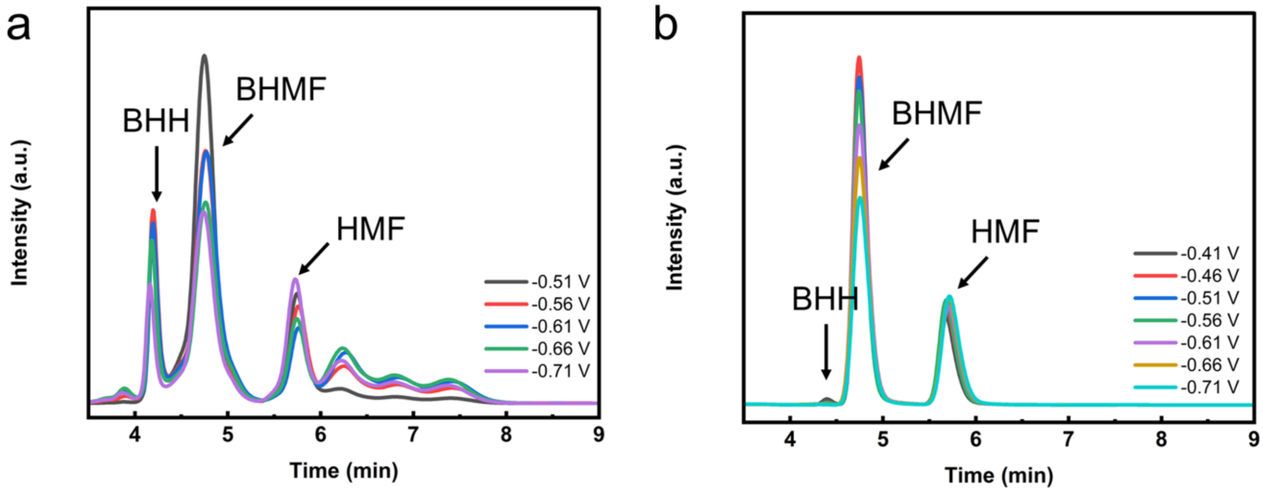

Fig. S13 HPLC profiles of the electrohydrogenation products catalyzed by (a) Ag foil and (b) PO-Ag NPs at various potentials in the electrolyte containing 50 mM HMF.

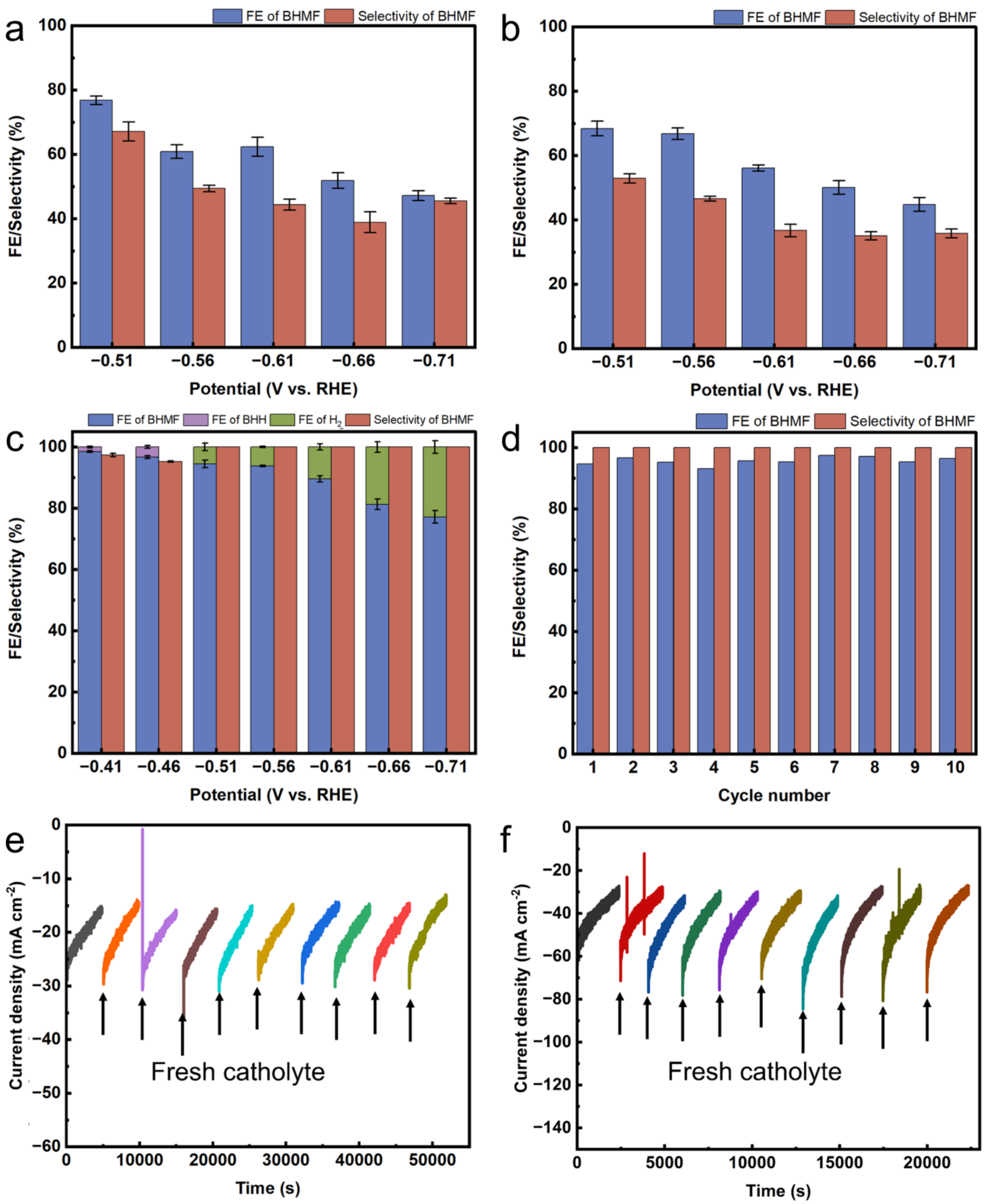

Fig. S14 FE and selectivity of BHMF for (a) 50 mM and (b) 100 mM HMF hydrogenation at different potentials using Ag foil as the working electrode. (c) FE and selectivity of BHMF for 50 mM HMF hydrogenation on a larger PO-Ag NPs (1 cm × 1 cm) at various potentials. (d) Recycling test of PO-Ag NPs (1 cm × 1 cm) for 50 mM HMF hydrogenation at −0.51 V vs. RHE. Stability test of PO-Ag NPs for HMF hydrogenation with sizes of (e) 1 cm × 1 cm and (f) 0.5 cm × 0.5 cm.

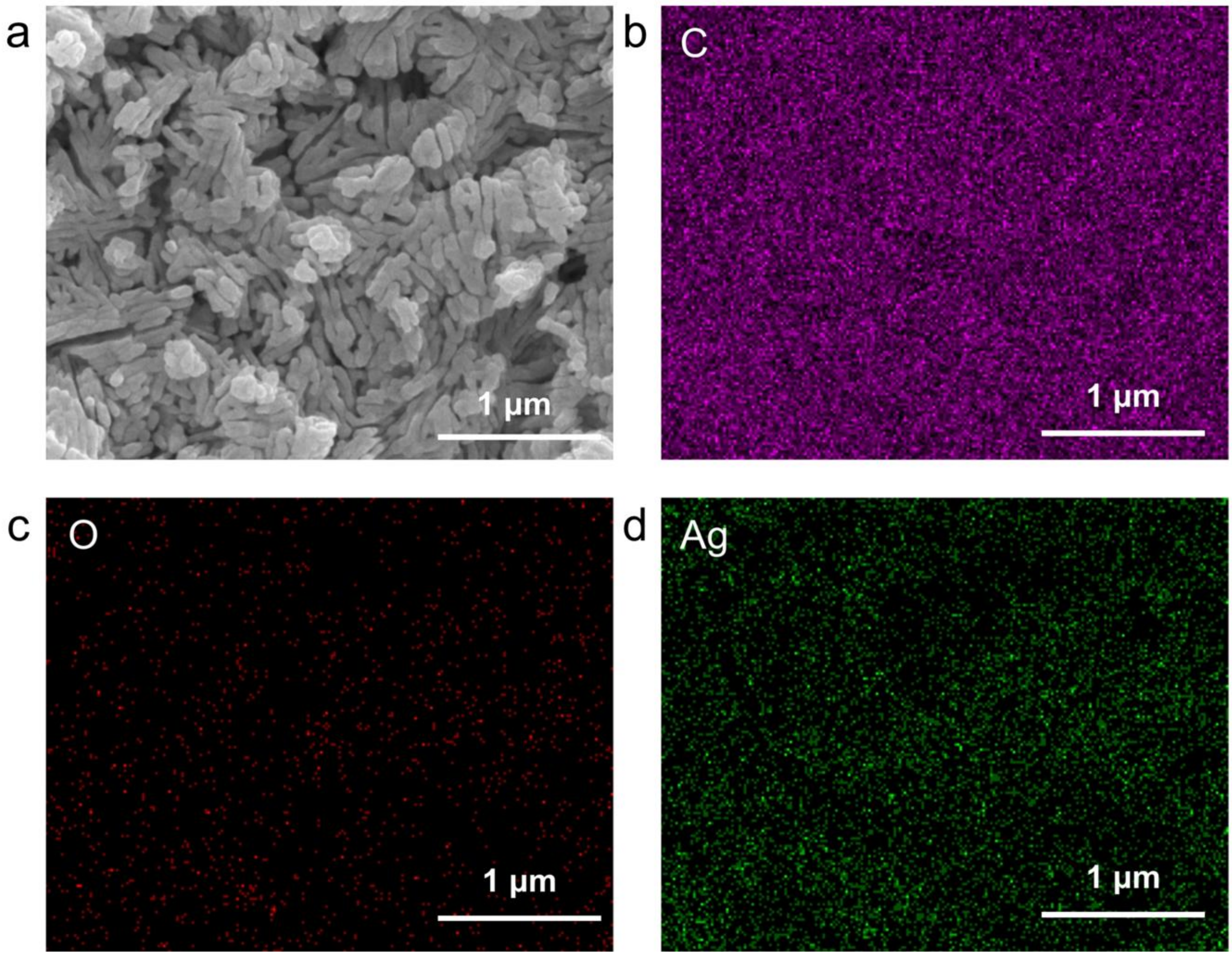

Fig. S15 (a) SEM image of PO-Ag NPs after electrolysis. (b-d) Corresponding elemental mappings.

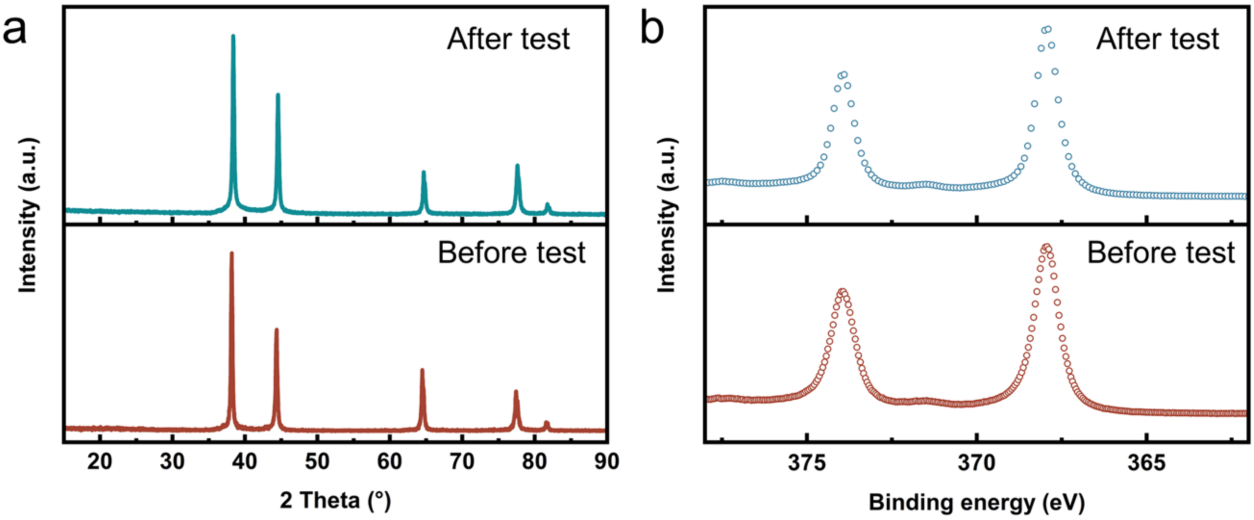

Fig. S16 (a) XRD patterns and (b) high-resolution Ag 3d XPS spectra of PO-Ag NPs before and after electrolysis.

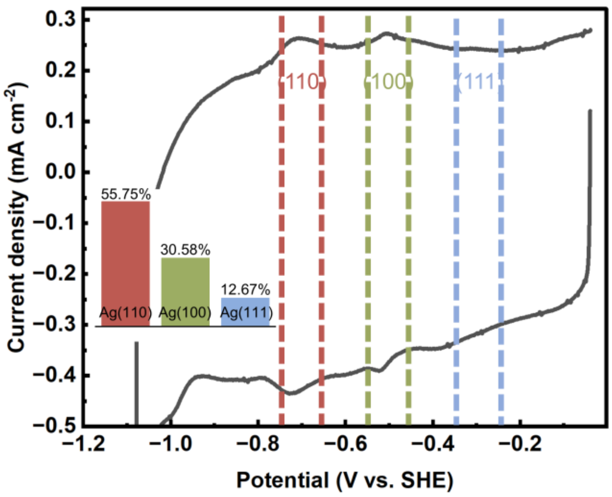

Fig. S17 CV curve of post-electrolysis of PO-Ag NPs in a 0.5 M $KHCO_3$ solution saturated with N_2 at a scan rate of 50 mV s^{-1} and the corresponding facet ratios obtained from HCO_3^- adsorption/desorption experiments.

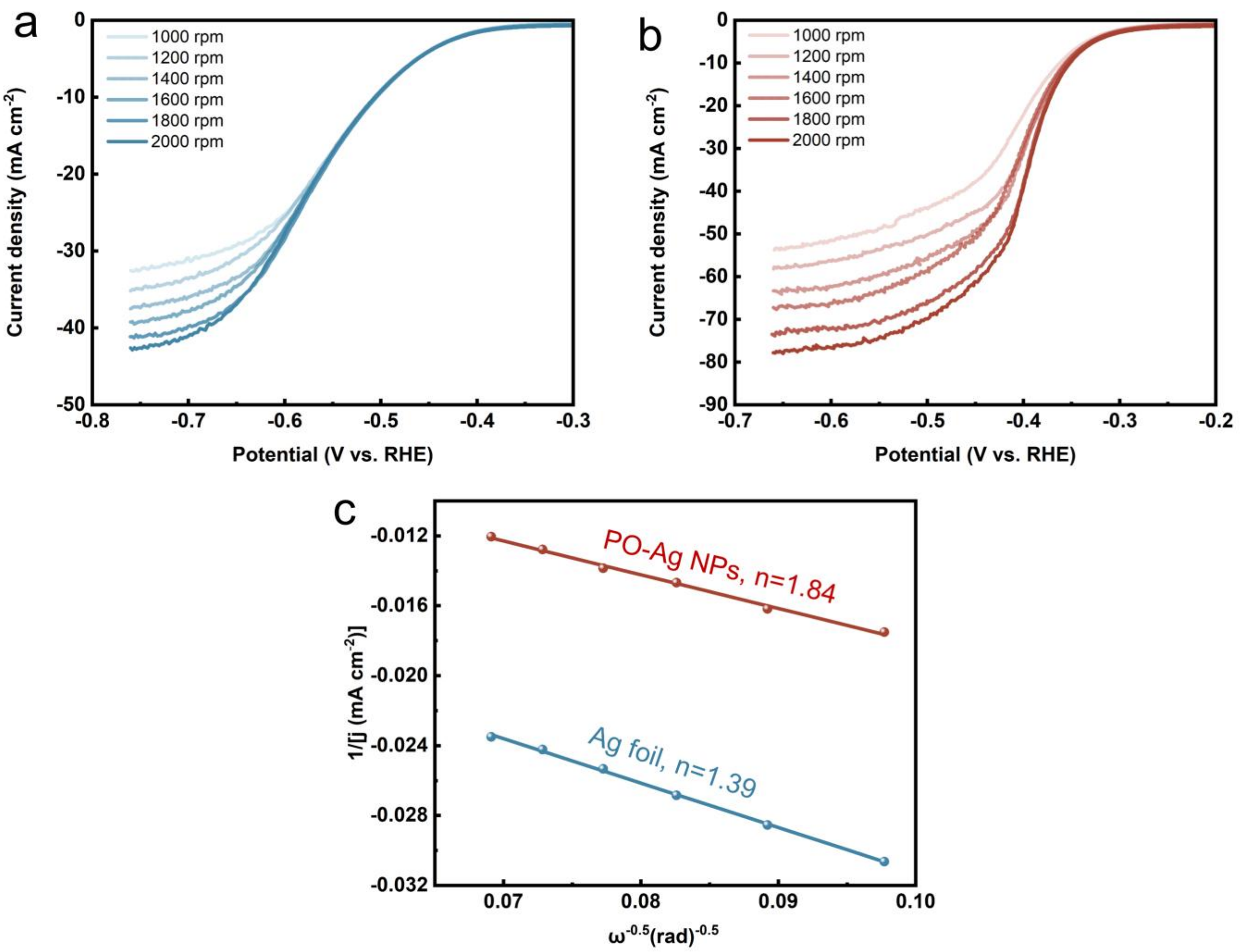

Fig. S18 LSV curves performed on RDE at different rotate rates with (a) Ag foil and (b) PO-Ag NPs as the working electrode. (c) Koutecký-Levich plots for Ag foil (blue line) and PO-Ag NPs (red line). The electron transfer number (n) was calculated by the equation of slope = $(0.62nFD^{2/3}\upsilon^{-1/6}C)^{-1}$.

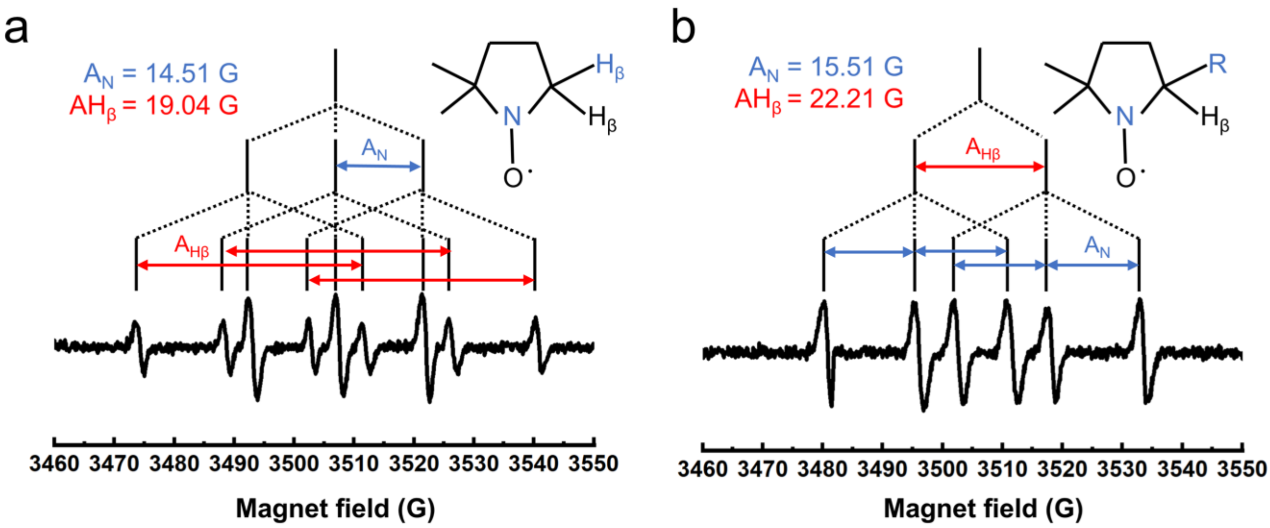

Fig. S19 The analysis of hyperfine splitting of DMPO adducts of (a) DMPO-H* and (b) DMPO-C*.

Table S1 Content of C and O in AD-Ag and PO-Ag NPs as determined by XPS.

Sample	C (Atomic %)	O (Atomic %)
AD-Ag	52.53	25.85
PO-Ag NPs	48.04	13.24

Table S2 Content of C and O in AD-Ag and PO-Ag NPs as determined by EDS.

Sample	C (Atomic %)	O (Atomic %)
AD-Ag	33.5	38.5
PO-Ag NPs	39.9	5.8

Table S3 Comparison of PO-Ag NPs with previous studies for HMF reduction.

Catalyst	**HMF concentration /Electrolyte**	**pH**	**Potential (V vs. RHE)**	**FE for BHMF (%)**	**Selectivity for BHMF (%)**	**BHMF Productivity (mmol cm^{-2} h^{-1})**	**Ref**
PO-Ag NPs	50 mM/1 M BBS	9.2	–0.46	96.1	93.7	0.529	This work
			–0.51	94	98	0.872	
	100 mM/1 M BBS	9.2	–0.51	91.2	94.1	0.915	
			–0.56	90.5	97.2	1.173	
Ag/C	20 mM/0.5 M BBS	9.2	–0.56	95	90	0.152	1
Ag/Cu foam	50 mM/0.5 M BBS	9.2	–0.51	85	83	0.180	2
	100 mM/0.5 M BBS	9.2	–0.51	70	68	0.100	
AgCu	20 mM/0.5 M BBS	9.2	–0.56	95	87	0.047	3
OD-Ag	20 mM/0.5 M BBS	9.2	–0.56	56.2	91.7	0.136	4
Ag$_{gd}$	20 mM/0.5 M BBS	9.2	–0.56	99	99	0.127	5
Ag/SnO$_2$	50 mM/0.5 M $KHCO_3$ solution	-	–0.62 to –1.12	> 95	-	0.704	6
CdPS$_3$/CdS	10 mM/0.1 M PBS	9.2	–0.7	91.3 ± 2.3	-	0.039	7
Ru$_1$Cu	50 mM/0.5 M PBS	7	–0.5	89.5	97	0.585	8
	100 mM/0.5 M PBS	7	–0.5	88	89.7	0.319	
Ag/Cu GD	50 mM/0.5 M BBS	9.2	–0.51	85	87	0.280	9
RhCu	50 mM/0.5 M Na_2SO_4 solution	-	-	92.6	-	0.340	10
Cu(OH)$_2$-ER/CF	5 mM/1 M KOH solution	14	–0.15	92.3	-	0.125	11
Ag@Cu NWAs/CF	20 mM/0.5 M BBS	9.2	–0.51	93.4	94.1	-	12

PBS: phosphate buffer solution

BBS: borate buffer solution

Table S4 Adsorption energy of HMF on Ag(111), Ag(100), and Ag(110) surfaces along with the aldehyde C=O bond lengths of adsorbed HMF.

	Adsorption energy (eV)	**Bond length of C=O (Å)**
HMF		1.228
Ag(111)	−0.853	1.241
Ag(100)	−0.873	1.246
Ag(110)	−0.985	1.251

Reference

1 X. H. Chadderdon, D. J. Chadderdon, T. Pfennig, B. H. Shanks and W. Li, *Green Chem.*, 2019, **21**, 6210-6219.

2 G. S. de Luna, P. H. Ho, A. Lolli, F. Ospitali, S. Albonetti, G. Fornasari and P. Benito, *ChemElectroChem*, 2020, **7**, 1238-1247.

3 L. Zhang, F. Zhang, F. C. Michel, Jr. and A. C. Co, *ChemElectroChem*, 2019, **6**, 4739-4749.

4 H. Liu, T.-H. Lee, Y. Chen, E. W. Cochran and W. Li, *Green Chem.*, 2021, **23**, 5056-5063.

5 Y. Kwon, K. J. P. Schouten, J. C. van der Waal, E. de Jong and M. T. M. Koper, *ACS Catal.*, 2016, **6**, 6704-6717.

6 X. Guo, H. Fu, J. Yang, L. Luo, H. Zhou, M. Xu, X. Kong, M. Shao, H. Duan and Z. Li, *ACS Catal.*, 2023, **13**, 13528-13539.

7 M. G. Sendeku, K. Harrath, F. T. Dajan, B. Wu, S. Hussain, N. Gao, X. Zhan, Y. Yang, Z. Wang, C. Chen, W. Liu, F. Wang, H. Duan and X. Sun, *Nat. Commun.s*, 2024, **15**, 5174.

8 K. Ji, M. Xu, S.-M. Xu, Y. Wang, R. Ge, X. Hu, X. Sun and H. Duan, *Angew. Chem. Int. Ed.*, 2022, **61**, e202209849.

9 G. S. de Luna, P. H. Ho, A. Sacco, S. Hernandez, J.-J. Velasco-Velez, F. Ospitali, A. Paglianti, S. Albonetti, G. Fornasari and P. Benito, *ACS Appl. Mater. Interfaces*, 2021, **13**, 23675-23688.

10 W. Zhang, Y. Qi, Y. Zhao, W. Ge, L. Dong, J. Shen, H. Jiang and C. Li, *Sci. Bull.*, 2023, **68**, 2190-2199.

11 M. Li, T. Zheng, D. Lu, S. Dai, X. Chen, X. Pan, D. Dong, R. Weng, G. Xu and F. Wang, *J. Energy Chem.*, 2023, **84**, 101-111.

12 Y. Zhong, R. Ren, Y. Peng, J. Wang, X. Ren, Q. Li and Y. Fan, *Mol. Catal.*, 2022, **528**, 112487.